IEIE Transactions on Smart Processing and Computing, vol. 4, no. 5, October 2015
http://dx.doi.org/10.5573/IEIESPC.2015.4.5.330

DWT-based Denoising and Power Quality Disturbance Detection

Muhammad Ramzan[1], and Sangho Choe[2]

[1] Department of Information, Communications, and Electronics Engineering, The Catholic University of Korea / Bucheon South Korea engr.ramzan009@gmail.com
[2] Department of Information, Communications, and Electronics Engineering, The Catholic University of Korea / Bucheon South Korea schoe@catholic.ac.kr

***** Corresponding Author: Sangho Choe

Received July 15, 2015; Revised August 11, 2015; Accepted August 29, 2015; Published October 31, 2015

***** *Regular Paper*

** Invited Paper: This paper is invited by Seung-won Jung, the associate editor.*

***** *Review Paper: This paper reviews the recent progress possibly including previous works in a particular research topic, and has been accepted by the editorial board through the regular reviewing process.*

** Extended from a Conference: Preliminary results of this paper were presented at the ITC-CSCC 2015. This present paper has been accepted by the editorial board through the regular reviewing process that confirms the original contribution.*

***Abstract*:** Power quality (PQ) problems are becoming a big issue, since delicate complex electronic devices are widely used. We present a new denoising technique using discrete wavelet transform (DWT), where a modified correlation thresholding is used in order to reliably detect the PQ disturbances. We consider various PQ disturbances on the basis of IEEE-1159 standard over noisy environments, including voltage swell, voltage sag, transient, harmonics, interrupt, and their combinations. These event signals are decomposed using DWT for the detection of disturbances. We then evaluate the PQ disturbance detection ratio of the proposed denoising scheme over Gaussian noise channels. Simulation results also show that the proposed scheme has an improved signal-to-noise ratio (SNR) over existing scheme.

***Keywords*:** Discrete wavelet transform (DWT), Power quality disturbances, Thresholding, Denoising, Detection

1. Introduction

Poor power quality (PQ) may cause some major problems to the use of the electronic equipment and furthermore may damage its efficiency and lifetime. The main reason of poor PQ is the disturbance events created along power line, such as voltage sag, voltage swell, voltage harmonics, voltage impulse, and interruption. There are a lot of PQ disturbance sources, such as adjustable speed drivers, electronic lamps blasts, power supplies, green energy devices like LED, and so on.

In smart grid (SG), power quality disturbance detection is a very big issue since various and incompatible power resources are connected together over the power grid. Voltage sags are caused by abrupt increase in load or source impedance. Voltage swells are induced by abrupt reduction in load, by lightening, faulting in circuits, or switching of capacitors. Harmonic current may be induced due to various non-linear loads. Also the fault clearing and utility switching often create various disturbances which degrade PQ. Hence, the mitigation of these disturbances becomes a big concern, even after the introduction of SG utilizing various kinds of power resources. Until now, for the PQ disturbance detection, Fourier transform (FT), short-term Fourier transform (STFT), neural networks (NN), and wavelet transform (WT) have been used. However, FT is not a reliable tool for the analysis of PQ events because it deals with only spectral information of signal such that the starting and ending time of PQ disturbances appearing along the time axis is not well monitored. Furthermore, FT does not work well for non-stationary signals like PQ disturbances [1]. STFT, also

called windowed FT, is reliable for stationary signals and overcomes the limitations of FT by segmenting the signal into narrow time intervals but cannot simultaneously provide good frequency and time resolutions [2]. NN is typically used with the WT, especially for the classification of disturbance patterns [3]. WT has two favorable characteristics over FT and STFT. First, WT allows simultaneous signal localization in time and frequency domain. Second, WT is able to separate the fine details representing transient signal components from coarse details such that the PQ disturbance detection is easily performed [4]. For the time frequency analysis of non-stationary signals, WT is more suitable because it provides time information along with spectral information. Discrete WT (DWT) is better for the PQ disturbance detection because it provides a flexible window where time-frequency variations are easily detectable. For the evaluation of the PQ detection, we generate various PQ disturbance signals including voltage sag, voltage swell, interruption, and the combined effect of sag-harmonics or swell-harmonics, on the basis of IEEE-1159 standard [5]. In this paper, we introduce a new DWT-based denoising technique and evaluate numerically the detection ratio of the proposed scheme.

The paper is organized as follows. In Section 2, we present the related work. In Section 3, we introduce the wavelet transforms and explain how to decompose a signal into different frequencies. Proposed signal denoising algorithm and PQ disturbance detection are presented in Section 4. Section 5 and Section 6 present numerical results of power quality disturbances and the detection ratio comparison with other schemes, respectively. Finally, Section 7 concludes our work.

2. Related Work

The extensive work has been pursued for the detection as well as analysis of PQ disturbances. Synchronization technique is used for the calculation and identification of the transient disturbances of PQ disturbances based on phased locked loop, but due to the distorted voltage the result may not be accurate [6]. In [7], by using windowing and interpolation the leakage and fence effect can be greatly reduced but the resolution is degraded greatly as well. Parabolic filter (PF) is used to remove background noise in 60 Hz (or 50Hz) power line interference, but in this technique, the ripples cause the loss in frequency content in the ECG signal [8]. The authors in [9] present an s-transform based technique, where the denoising threshold can be determined with the energy congregation level (ECL). In [10, 11], the authors apply a new wavelet denoising approach to the electrocardiogram (ECG) signal. Compared to the above-mentioned other schemes, the WT offers relatively a good frame for the analysis of the PQ disturbance signals in which signal energy can be localized both in time & scale domain. Hence, the multi-resolution analysis that is based on WT is a great tool providing spatial frequency decomposition [12]. Some literatures [13-19] present wavelet thresholding-based schemes that remove the PQ disturbances. Among them, the authors in [15], very recently, suggest a DWT-based noise removal scheme using correlation that improves the PQ event detection ratio. The authors in [20] suggest a multilevel thresholding-based wavelet denoising method, which may compensate the deficiency of soft- and hard-thresholding.

3. Wavelet Transform

WT looks similar to FT but has different merits in it. WT is well applicable to non-stationary signals like images, sound signals, and PQ signals. WT decomposes the signal on the basis of dilated and translated wavelets. After the decomposition & synthesis process, the original signal can be recovered without losing any information.

We briefly explain WT and inverse WT (IWT) [13-18] as follows. On the WT process, while the time resolution increases for the high frequency portion, the frequencies localization increases for the low frequency portion. After applying the dilations and translations to the mother wavelet $\psi(t)$, the daughter wavelet is

$$\psi_{a,b}(t) = |a|^{-\frac{1}{2}} \psi\left(\frac{t-b}{a}\right), \tag{1}$$

where a is the scaling factor and b is the translating factor. The continuous WT (CWT) of the signal $x(t)$ with wavelet $\psi(t)$ can be written as

$$CWT_x(a,b) = |a|^{-\frac{1}{2}} \int_{-\infty}^{\infty} x(t)\psi^*\left(\frac{t-b}{a}\right)dt, \tag{2}$$

where $(\cdot)*$ indicates the complex conjugate of $(\cdot)$. FT of (1) is shown below

$$\hat{\psi}_{a,b}(\omega) = |a|^{-\frac{1}{2}} \int_{-\infty}^{\infty} \psi\left(\frac{t-b}{a}\right) e^{-j\omega t}dt. \tag{3}$$

For practical applications, we can convert CWT into discrete WT (DWT) with the sampled version x_n of $x(t)$. The dyadic WT can be defined as:

$$DWT_x(m,n) = |2|^{-\frac{m}{2}} \int_{-\infty}^{\infty} x_k\psi^*\left(\frac{k-n}{2^m}\right)dt, \tag{4}$$

where k is an operating index, m is a scaling number, and $n = 1, 2, \ldots N$ (where N is the number of sampling points). In (4), we can see that factors a and b of (2) are translated into integer parameters m and n with $a = 2^m$ and $b = n$. First, for $m = 1$, the wavelet filtering operation extracts the first scale wavelet coefficients (WCs) that are the highest frequency components of signal x. Then, as m increases, i.e., 2, 3, …, the filtering operation extracts the 2nd, 3rd, …, scale WCs, i.e., the 2nd, 3rd, …, highest

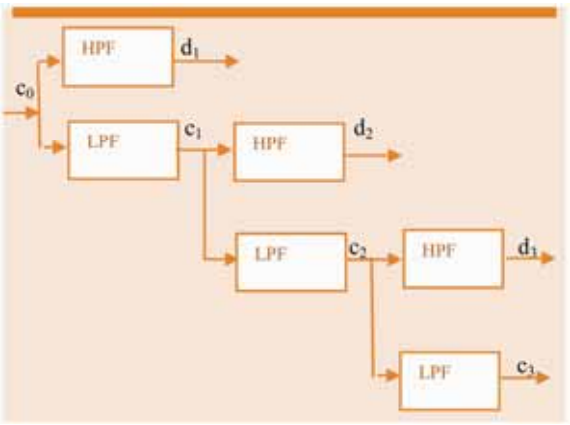

Fig. 1. Decomposition of signal by using WT.

frequency components of signal x. As mentioned earlier, since diverse frequency components often exist in disturbing disturbance signals, the investigation of WTCs at the different scales would help to determine the occurrence of the disturbing events as well as their occurring times.

In this paper, we perform a multi-resolution decomposition using dyadic DWT. The $c_0(t)$ (that is the sampled version of input signal $x(t)$ as seen in (5)) is decomposed into detailed signals by high pass filter (HPF) $g(t)$ and approximate signals by low pass filter (LPF) $h(t)$. At first scale $m=1$, the detailed signal contains high frequency components having sharp edges and transitions (like PQ disturbance) and the approximate signal includes low frequency components.

$$c_1(n)=\sum_k h(k-2n)c_0(k) \tag{5}$$

$$d_1(n)=\sum_k g(k-2n)c_0(k) \tag{6}$$

$$c_l(n)=\sum_k h(k-2n)c_{l-1}(k) \tag{7}$$

$$d_l(n)=\sum_k g(k-2n)c_{l-1}(k) \tag{8}$$

Note that after the decomposition process at the lth (= 1, 2, 3 …) stage, the length of the two decomposed (output) signals, c_l and d_l, would be half of one of the input signal c_{l-1} [14].

4. Proposed Algorithm for Signal Denoising and PQ Disturbance Detection

In this section, we present a denoising algorithm removing noise from power line signal such that reliable PQ disturbance detection would be possible. The proposed denoising algorithm is briefly explained in Fig. 2, where

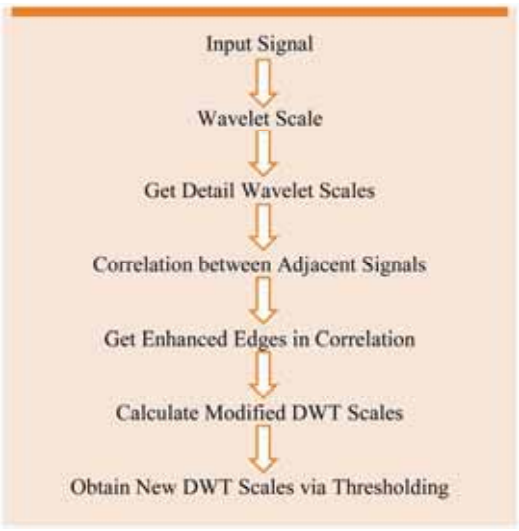

Fig. 2. DWT-based denoising algorithm.

shows that the PQ disturbances can be accurately detected through the denoising process. In this algorithm, we decompose an input signal and then remove the noise components from the signal for the PQ disturbance detection. The original signal can be recovered by applying inverse discrete wavelet transform (IDWT) to the output signal of the noise removal process.

As an example, Fig. 3 shows a noisy voltage sag signal (i.e., input signal seen in Fig. 3(a)) and its intermediate results obtained through the presented noise removal process. In that noisy input signal, the voltage sag makes the RMS of original signal starting near 0.03 sec and ending near 0.06 sec dropped to 15%. The sampling rate is set at 15360 points/s (i.e., the average sampling points of 256 in each cycle) and the signal-to-noise ratio (SNR) is assumed to be 35 dB.

We present a DWT-based noise removal algorithm using a modified correlation thresholding whose detail procedure is given as follows.

Step1: Calculate the correlation between the adjacent scales as follows:

$$\begin{aligned} Corr_k(m,\ n) &= DWT_x(m\ \ n) \\ &\quad DWT_x(m+1,n)\ \ \ldots\ DWT_x(m+k-\ \ n) \\ &= \prod_{i=0}^{k-1} DWT_x(m+i,n), \\ &\quad s.t.\ \ m < M-k+ \end{aligned} \tag{9}$$

where n =1, 2, 3, ..., N is the sampling point, N is the number of sampling points, k is the number of scale inter-multiplication (• denotes the scale inter-multiplication operator), and M is the number of all scales. Hereinafter, for simplicity, we assume k = 2 and m = 1; however, in terms of detection ratio and complexity, the numerical results show that k = 2 is better than $k \geq 3$ (see Table 7 in Section 6).

Though the DWT process for a noisy voltage sag signal (see Fig. 3(a)), we obtain the first scale $DWT_x(1,\ n)$ and

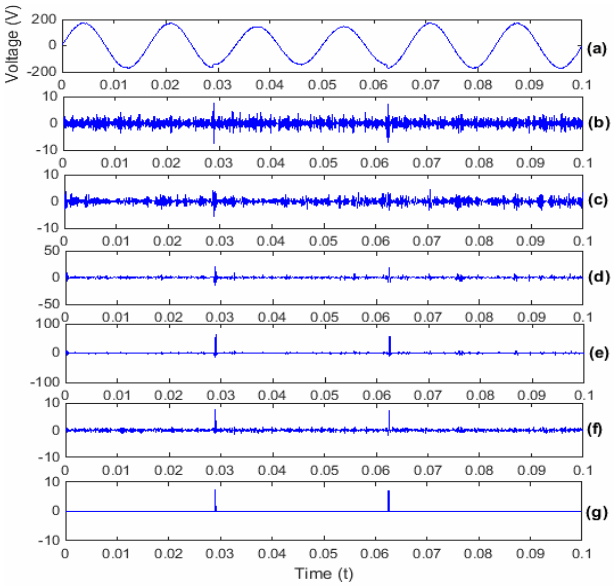

Fig. 3. The proposed noise removal algorithm. (a) Voltage sag with noise, (b), (c) WTC's at scales 1 and 2 respectively, (d) correlation between (b) & (c), (e) modified correlation, (f) partially modified first scale, (g) denoised new first scale.

the second scale $DWT_x(2, n)$, which are seen in Fig. 3(b) and (c) respectively. Using the correlation function $Corr_2(1, n) = DWT_x(1, n)\ DWT_x(2, n)$ (see Fig. 3(d)), we can enhance the amplitude at the edge points of the disturbance signal while suppressing the one of the background noise signal. That is, the two edges (starting and ending points of the disturbance signal) are much sharper and stronger in the correlation $Corr_2(1, n)$ than in the scales $DWT_x(m, n)$. From Fig. 3(d), we can also observe that noise components are almost negligible at a localized region compared to disturbance signal components such that the noisy background removal from x using correlation instead scales is relatively easier [15]. It implies that the direct spatial correlation over k different scales, $Corr_k(1, n)$, may improve the accuracy of locating important edges due to PQ events [22].

Step 2: In this step, we further strengthen the starting and ending edges representing the disturbance using a modified correlation, denoted as $Corr_{modified,k}(m, n)$. After finding the starting and ending positions, we multiply these two points of disturbances with S (which is the mean value of $Corr_k(m, n)$). For the same previous example with $k = 2$ and $m = 1$, multiplication of these two main points with S gives the modified correlation value $Corr_{modified,2}(1, n)$, which is shown in Fig. 3(e). In Fig. 3(e), we can observe that the two main edges (representing the starting and ending points of disturbance) in $Corr_{modified,2}(1, n)$ are more prominent than the ones in $Corr_2(1, n)$; it implies that we could further suppress the background noise components using $Corr_{modified,2}(1, n)$ than $Corr_2(1, n)$.

Step 3: This step calculates the partially-modified scale (PMS) $DWT_{p.modified,x}(m, n)$ as follows:

$$DWT_{p.modified,x}(m, n) = \frac{Corr_{modified,k}(m, n)}{S*DWT_x(m+1, n)} \tag{10}$$

where $*$ denotes the scalar multiplication. The PMS enhances the edges of disturbance and reduces the noise more as compared to $DWT_x(m, n)$ or $Corr_k(m, n)$. For the same previous example, the PMS can be derived as

$$DWT_{p.modified,\ x}(1, n) = \frac{Corr_{modified,2}(1, n)}{S*DWT_x(2, n)}$$

We can see that the PMS, whose diagram is seen in Fig. 3(f), clarifies the two edges of the disturbance such that the more exact thresholding value can be obtained (see the next step).

Step 4: Naturally, in the threshold based algorithm, it is very critical to determine the threshold value. Donoho et al. [21] present a universal threshold in their well-known wavelet shrinkage scheme as follows:

$$THR(m) = \sigma_{SD}\sqrt{2\log N} \tag{11}$$

where Donoho et al. [21] estimate the Gaussian noise standard deviation: $\sigma_{SD}(m) = median\ (wavelet\ scales)/.6745$.

In the proposed scheme, we suggest a modified correlation thresholding, where the standard deviation $\sigma_{SD}(m)$ in (11) is defined as

$$\sigma_{SD}(m) = \frac{median\left(DWT_{p.modified,\ x}(m,n)\right)}{0.6745}.$$

For the previous example, putting the value of $DWT_{p.modified,\ }(1, n)$ in (11) gives $THR(1)$ which helps to find new scale $DWT_{new,x}(1, n)$. By the comparison of $DWT_{p.modified,\ x}(m, n)$ and threshold value $THR(m)$, we can calculate the masking value. The pseudo-code expression that defines the masking value is given as:

For $m = 1 : M$
  For $n = 1 : N$ #
    If $DWT_{p.modified,\ x}(m, n) < THR(m)$
    Then $MASK(m, n) =$
    Else $MASK(m, n) =$
  End
End

Note that the main edges can be extracted by comparing $DWT_{p.modified,x}(m, n)$ and $THR(m)$; if the coefficients of $DWT_{p.modified,x}(m, n)$ are less than $THR(m)$ then the masking value will be 0, otherwise it will be 1. Next step calculates new DWT scales using the masking value.

Step 5: This step calculates new wavelet scales as follows:

$$DWT_{new,x}(m, n) = MASK(m,n)\,DWT_x(m, n).$$

This operation effectively removes noise such that the starting and ending points of disturbance become prominent. Fig. 3(g) shows the noise-removed first scale $DWT_{new,x}(1, n)$ with prominent disturbance edges. We use the inverse discrete wavelet transform (IDWT) in order to reconstruct the original signal where we can check the recovered SNR gain representing how much signal quality is improved. Numerical results show that the presented scheme achieves the recovered SNR gain of up to 6 dB over the typical channel environments (see Section 6).

5. Numerical Results

In this section, for the detection analysis of PQ disturbances, we generate voltage sag, voltage swell, interruption, harmonics, and the combined effect of sag & interruption or sag & harmonics, on the basis of IEEE-1159 standard. Using a Matlab simulation, we evaluate the PQ disturbances over different channel conditions in terms of SNR, numbers of disturbance cycles, and so on. Via the simulation, we can confirm that the proposed technique improves PQ disturbance detection ratio compared to the previous scheme [15]. Using the parameters in Table 1, we could generate various disturbance signals for testing.

5.1 Voltage Sag

By abrupt load change like motor start, short circuit, and loose connection, the root-mean-square (RMS) value of power signal could be decreased for a short amount of interval that is known as voltage sag or voltage dip. A voltage sag event happens when the input signal reduces

Table 1. Signal model and their parameters.

PQ disturbance	Model	Parameters
Sine-Wave	$x(t) = A\sin(\omega t)$	$A = 1$
Sag	$x(t) = A(1-a(u(t-t_1)-u(t-t_2)))$ $t_1< t_2$, $u(t) = 1$, $t\geq 0$	$0.1< a \leq 0.9$ $T\leq t_2-t_1 \leq 8T$
Swell	$x(t) = A(1+a(u(t-t_1)-u(t-t_2)))$ $t_1< t_2$, $u(t) = 1$, $t \geq 0$	$0.1< a \leq 0.8$ $T\leq t_2-t_1 \leq 8T$
Harmonics	$x(t) = A[\sin(\omega t)+a_3\sin(3\omega t)$ $+a_5(5\omega t)]$	$0.1\leq a_3 \leq 0.2$ $0.05\leq a_5 \leq 0.5$
Interruption	$x(t) = a[1-a(u(t-t_1)-u(t-t_2))]$ $\sin(\omega t)$	$0.1\leq \beta \leq 0.2$ $0.05\leq \gamma \leq 0.1$

Table 2. Types of sag voltage.

Types of Sag (As per IEEE standards)		
Types	**Time Duration**	**Typical Amplitude**
Momentaneous Sag	30 Cycles to 3 Sec	0.1-0.9 p.u
Temporary Sag	3 sec to 1 min	0.1-0.9 p.u
Long-term under	>1min	0.8-0.9 p.u
C1→Pure sinusoidal, C3→Temporary Sag, C2→Momentory Sag, C4→long-term sag		

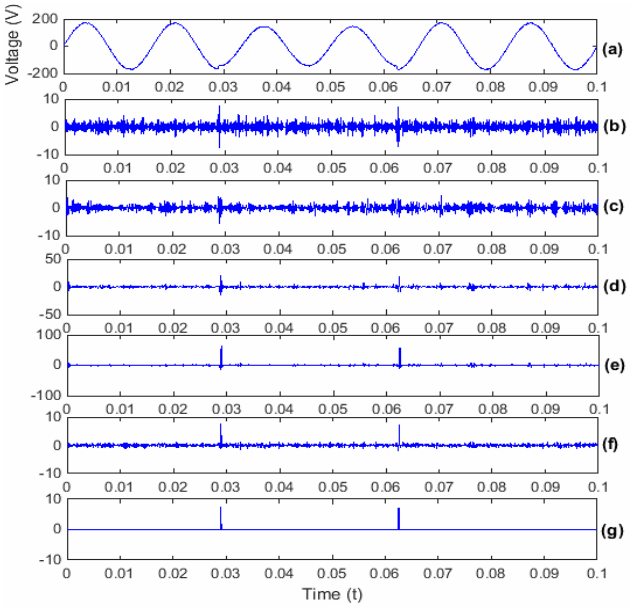

Fig. 4. (a) Voltage sag with noise, (b), (c) WTC's at scales 1 and 2 respectively, (d) correlation between (b)&(c), (e) modified correlation, (f) partially modified first scale, (g) denoised new first scale.

10 to 90 % of the standard RMS value (220V/110V). Table 2 shows different kinds of voltage sag defined by the IEEE standard [5].

The signal shown in Fig. 4(a) includes a 15 % momentaneous sag. Fig. 4(d) displays the correlation results between the details scales $DWT_x(1, n)$ seen in Fig. 4(b) and $DWT_x(2, n)$ seen in Fig. 4(c). Fig. 4(e) and (f) show the modified correlation $Corr_{modified,2}(1, n)$ and PMS $DWT_{p.modified,}(1, n)$, respectively. After going through the proposed procedure, the resulted new scale $DWT_{new,x}(1, n)$ in Fig. 4(g) shows almost noiselessly enhanced disturbance points. Two main edges clearly shows the presence of the voltage sag event.

5.2 Voltage Swell

According to the IEEE standard, a voltage swell event happens when the RMS value of the original signal increases from 10 to 90 % at the power frequency with the duration of 1/2 cycles to 60 seconds. Table 3 shows voltage swell signals defined by the IEEE standard [5].

Table 3. Types of voltage sag.

Voltage Swell	Magnitude	Duration
Instantaneous	1.1 to 1.8 pu	0.5 to 30 cycles
Momentary	1.1 to 1.4 pu	30 cycles to 3 sec
Temporary	1.1 to 1.2 pu	3 sec to 1 min

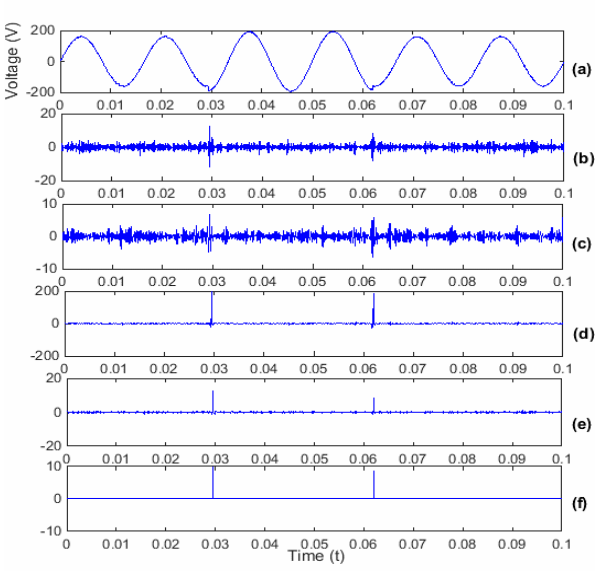

Fig. 5. (a) Voltage swell with noise, (b), (c) WTC's at scales 1 and 2 respectively, (d) modified correlation, (e) partially modified first scale, (f) denoised new first scale.

The instantaneous voltage swell signal, shown in Fig. 6(a), has 15 % swell that is used for numerical results.

Fig. 5(b) and (c) indicate the details scales $DWT_x(1, n)$ and $DWT_x(2, n)$, respectively, and Fig. 5(d) and (e) show the modified correlation scale $Corr_{modified,2}(1, n)$ and the PMS $DWT_{p.modified,x}(1, n)$, respectively. Fig. 5(f) shows the updated (new) first scale $DWT_{new,x}(1, n)$ that has prominent disturbance points.

5.3 Transient Harmonics

Due to non-linear electric loads, the harmonics voltages or currents can be created automatically in electric power systems. In Fig. 6(a), a harmonics signal generated in a range of 0.03 to 0.05 seconds is shown. Fig. 6(b) and (c) display the first and second detail scales $DWT_x(1, n)$ and $DWT_x(2, n)$, respectively, and Fig. 6(d) and (e) show the modified correlation $Corr_{modified,2}(1, n)$ and the PMS $DWT_{p.modified,x}(1, n)$ Via the proposed procedure, the obtained new scale $DWT_{new,x}(1, n)$ has the clear PQ detection point as shown in Fig. 6(f).

5.4 Interruption

According to the IEEE 1159 standard, in the case of

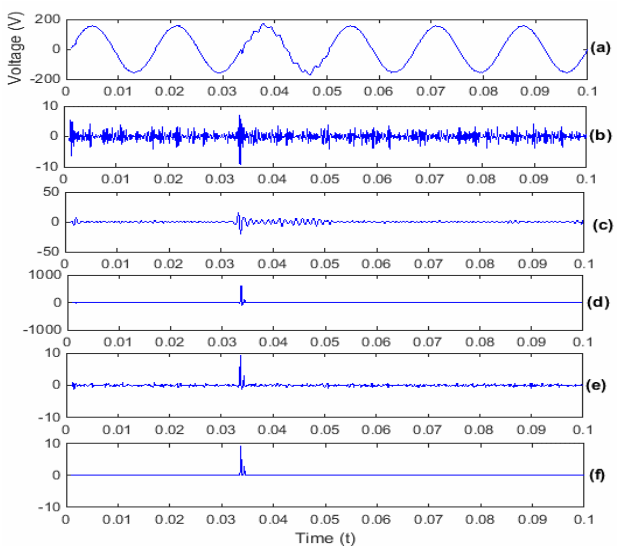

Fig. 6. (a) noisy voltage harmonics signal, (b), (c) WTC's at scales 1 and 2 respectively, (d) modified correlation, (e) partially modified first scale, (f) denoised new first scale.

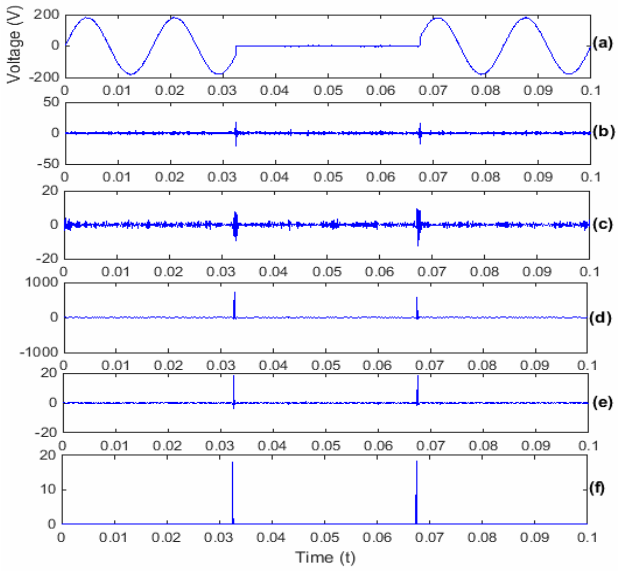

Fig. 7. (a) Voltage noisy interruption signal. (b), (c) WTC's at scales 1 and 2 respectively, (d) modified correlation. (e) partially modified first scale, (f) denoised new first scale.

interruption, voltage magnitude is always less than 10 % of nominal value. Generally, interruption severely affects the industrial areas, including the continuous process industry and the communication and information processing business. An interruption signal, along with noise, is shown in Fig. 7(a). Fig. 7(b) and (c) display the detail scales $DWT_x(1, n)$ and $DWT_x(2, n)$, respectively, and Fig. 7(d) and (e) show the modified correlation $Corr_{modified,2}(1, n)$ and PMS $DWT_{p.modified,x}(1, n)$. The resulted $DWT_{new,x}(1, n)$ shows the two distinguishable main disturbance points.

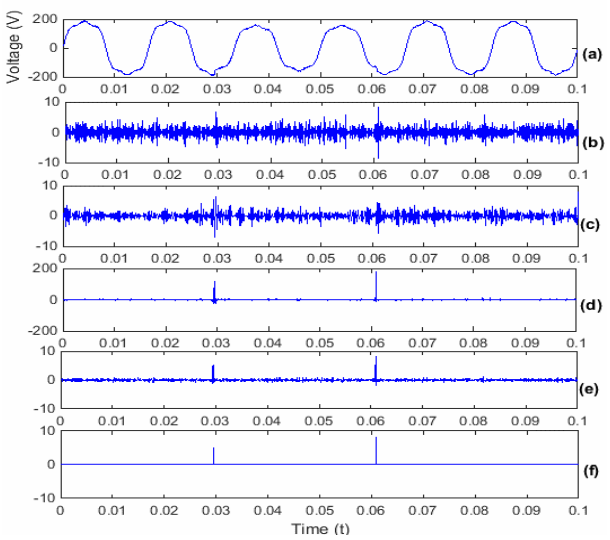

Fig. 8. (a) Voltage noisy sag-harmonics signal, (b), (c) WTC's at scales 1 and 2 respectively, (d) modified correlation, (e) partially modified first scale, (f) denoised new first scale.

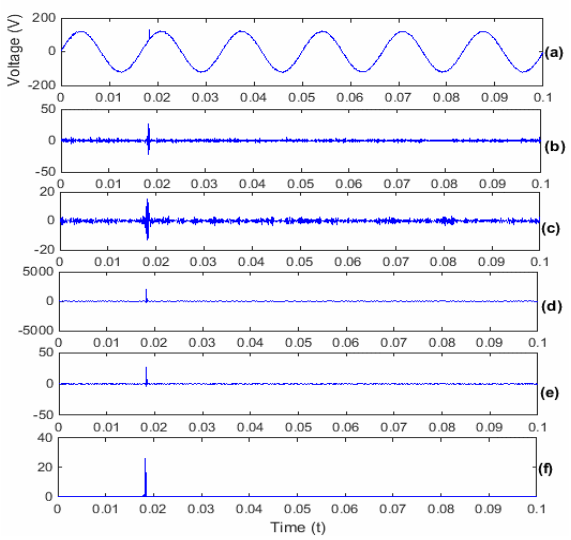

Fig. 10. (a) Voltage noisy impulse case, (b), (c) WTC's at scales 1 and 2 respectively, (d) modified correlation, (e) partially modified first scale, (f) denoised new first scale.

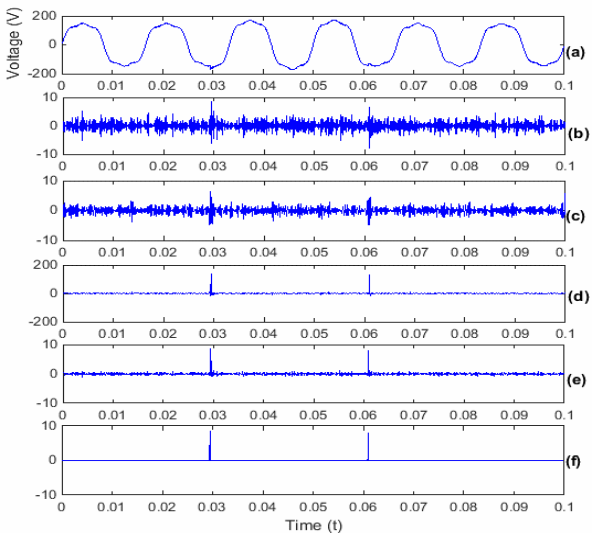

Fig. 9. (a) Voltage noisy swell-harmonics signal. (b), (c) WTC's at scales 1 and 2 respectively, (d) modified correlation, (e) partially modified first scale, (f) denoised new first scale.

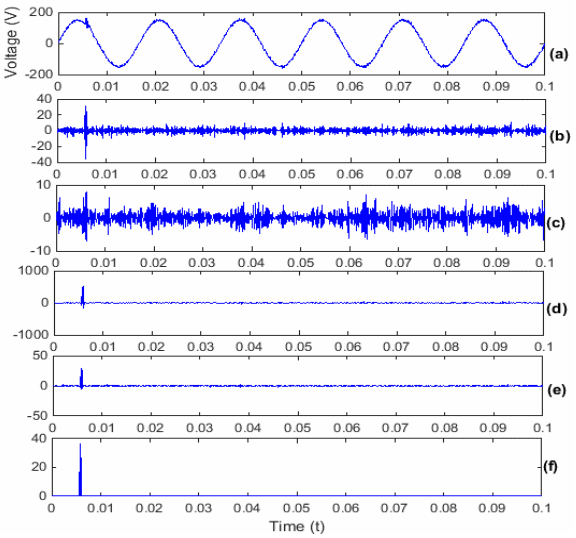

Fig. 11. (a) Voltage noisy high frequency case, (b), (c) WTC's at scales 1 and 2 respectively, (d) modified correlation, (e) partially modified first scale, (f) denoised new first scale.

5.5 Sag-Harmonics and Swell-Harmonics

In this section, the combined effect of sag harmonics and swell harmonics disturbance is analyzed. There is a 15 % sag signal along with harmonics that are shown in Fig. 8(a). Fig. 8(b) and (c) are the detail scales $DWT_x(1, n)$ and $DWT_x(2, n)$, respectively, and Fig. 8(d) and (e) are the modified correlation $Corr_{modified,2}(1, n$ and the PMS $DWT_{p.modified,\ x}(1, n)$, respectively. Fig. 8(f) shows the new first scale $DWT_{new,x}(1, n)$ that has the prominent disturbance points.

Fig. 9 shows the denoising and detection of a combined disturbance signal with swell and harmonics. After going through the proposed scheme, the resulting new scale $DWT_{new,x}(1, n)$ in Fig. 9(f) shows the enhanced disturbance points.

5.6 Voltage Impulse and High Frequency Transient

Following the IEEE standard, we generate a voltage impulse at 0.02 sec as shown in Fig. 10(a). Fig. 10(b) and (c) plot the detail scales $DWT_x(1, n)$ and $DWT_x(1, n)$, and Fig. 10(d) and (e) show the modified correlation $Corr_{modified,2}(1, n)$ and PMS $DWT_{p.modified,x}(1, n)$, respectively. Fig. 10(f) shows the new scale value

Table 4. Detection ratio comparison of proposed algorithm and previous algorithm [15].

SNR(dB)		Detection Ratio of Different Disturbances				
SNR1	SNR2	Sags	Swells	Interrup-tion	Har-monics	Impulse
50	51.9	100 (100)	100 (100)	100 (100)	100 (100)	100 (100)
45	49.2	100 (100)	100 (100)	100 (100)	100 (100)	100 (100)
40	45.3	100 (98)	100 (97)	100 (96)	100 (100)	100 (98)
35	40.1	100 (96)	100 (94)	100 (92)	100 (100)	100 (96)

$DWT_{new,x}(1, n)$ that has the two main disturbance edges indicating presence of that PQ disturbance.

High frequency transient (HFT) is one of the PQ disturbances that evaluates the quality of the electrical power. In Fig. 11, we apply the proposed scheme to the noisy HFT signal to remove the noise. Two main edges shown in Fig. 11(f) verifies the presence of the HFT-based PQ disturbance.

6. Detection Ratio of Power Quality Disturbances

Using Matlab, we numerically evaluate the detection ratio of PQ disturbance at the different SNR with a range of 50 to 35 dB, which vary the level of noise accordingly. The detection ratio and the recovered SNR gain (= SNR2 [= recovered output SNR] – SNR1 [= input SNR]) of the proposed scheme are listed in Table 4 and compared to the ones (see the bracketed values (·) in Table 4) of existing scheme in Ref. [15].

For each PQ disturbance alluded in Section 5, we create a total of 100 statistically-independent test sample sets (or test signals). For further validation of the calculated detection ratio, for each disturbance event, we generate the signals with different number of disturbance cycles (i.e. 20, 10, and 5). In Table 4, we can observe that the proposed scheme improves the detection ratio for all the disturbances, especially at low SNR (≤ 35 dB), compared to exiting scheme [15]. Table 4 also shows that the SNR gain of the presented scheme is about 5 to 6 dB for SNR1 = 35dB or 40dB and 2 dB for SNR1 = 50dB, respectively.

Table 5 shows the statistically-evaluated (and selectively chosen) false alarm rate R_{fa} (Type I error rate) and miss detection rate R_{md} (Type II error rate; which is shown in brackets) of the proposed scheme for different disturbance events. From Table 5, it is noticeable in terms of test reliability that both R_{fa} and R_{md} are less than 0.3%. Furthermore, the proposed scheme without a convergence loop has lower complexity than the existing scheme with a convergence loop [15].

We can also calculate the detection ratio of the proposed scheme by taking different number of disturbance cycles (i.e. 20, 10 and 5) which is listed in Table 6. We confirm that for 35 dB SNR1, the detection ratio decreases as the number of cycles is less than 5.

Table 5. Statistically-evaluated false alarm and miss detection rate (%) of proposed scheme.

	R_{fa} (%) & R_{md} (%)				
SNR1	Sags	Swells	Interrup-tion	Har-monics	Impulse
50	0.2602 (0)	0.2589 (0)	0.2602 (0)	0.3333 (0)	0.2642 (0)
45	0.1301 (0)	0.1301 (0)	0.2602 (0)	0.3317 (0)	0.2596 (0)
40	0.1301 (0)	0.1301 (0)	0.2069 (0)	0.3000 (0)	0.1327 (0)
35	0.1258 (0.56)	0.1176 (0.82)	0.1301 (0.03)	0.2283 (0.67)	0.1301 (0)

Table 6. Detection ratio of proposed scheme at different disturbance cycles.

Cycles	SNR1	Detection ratio of different disturbance		
		Sags	Swells	Harmonics
20	35 ~ 50	100	100	100
10	35 ~ 50	100	100	100
5	40 ~ 50	100	100	100
5	35	97	94	98

Table 7. Detection ratio comparison of $Corr_2$ and $Corr_3$.

SNR(dB)		Detection ratio of Different Disturbances			
SNR1	SNR2	Sags	Swells	Interrup-tion	Har-monics
50	51.91	100 (100)	100 (100)	100 (100)	100 (100)
45	49.22	100 (100)	100 (100)	100 (100)	100 (100)
40	45.39	100 (98)	100 (97)	100 (100)	100 (100)
35	40.12	100 (88)	100 (84)	100 (90)	100 (92)

Table 7 compares the detection ratio of the proposed scheme with the two different scales: $Corr_2$ with $k = 2$ (non-bracketed values) and $Corr_3$ with $k = 3$ (bracketed values). It is observable that the detection ratio of $Corr_3$ is less than one of $Corr_2$, especially when SNR1 = 35 or 40 dB. Since $Corr_2$ is relatively simple but has comparable performance, it is used throughout the paper.

7. Conclusion

In this paper, we have proposed a new denoising technique that improves the PQ disturbance detection ratio. The proposed approach effectively removes the additive noise along the power line such that the reliable PQ

disturbance detection is achievable. Simulation results verify that the presented DWT-based algorithm is an efficient tool for the detection of PQ disturbance signal having inherently non-stationary piecewise-linear behavior. Specifically, the recovered SNR gain of the presented scheme is 5 to 6dB at the range of 35 to 50 SNR and its detecting rate is superior to existing scheme, especially at low SNR (35 to 40 dB). For future work, we will analyze the robustness of denoising algorithm theoretically as well as numerically.

Acknowledgement

This research was supported by the National Research Foundation of Korea (NRF) grant funded by the Korean government (MEST) (No. 2011-0015286)

References

[1] S. Santoso, W. M. Grady, E. J. Powers and J. Lamoree, "Characterization of distribution power quality events with Fourier and wavelet transforms" IEEE Tras. Power Delivery, vol. 15, pp. 247-254, Jan 2000. Article (CrossRef Link)

[2] G. T. Hyydt, P. S. Fjeld, C. C. Liu, D. Pierce, L. Tu and G, Hensley, "Application of the windowed FFT to electric PQ assessment" IEEE Tran. Power Delivery, vol. 14, pp. 1411-1416, Oct. 1999. Article (CrossRef Link)

[3] W. Liao, H. Wang and P. Han, "Neural network-based detection and recognition method for power quality disturbances signal" Conf. Control and Decision, Xuzhou, China, pp. 1023-1026, May 2010. Article (CrossRef Link)

[4] M. Sifuzzaman, M. R. Islam and M. Z. Ali, "Application of wavelet transform and its advantages compared to Fourier transform," Journal of Physical Sciences, vol. 13, no. 1, 2009, pp. 121-134. Article (CrossRef Link)

[5] IEEE Working Group P1159, "Recommended practice monitoring electric power quality –Draft 7", Dec. 1994. Article (CrossRef Link)

[6] Antonio Cataliotti, Valentina Cosentino, and Salvatore Nuccio, "A phase- locked loop for the synchronization of power quality instruments in the presence of stationary and transient disturbances" IEEE Transactions On Instrumentation And Measurement, Vol. 56, No. 6, December 2007. Article (CrossRef Link)

[7] Surya Santoso, W. Mack Grady, Edward J. Powers, Jeff Lamoree and Siddharth C. Bhatt, "Characterization of distribution power quality events with Fourier and wavelet transforms" IEEE Transactions On Power Delivery, Vol. 15, No. 1, January 2000. Article (CrossRef Link)

[8] G. Kavya and Dr. V. Thulasibai, "Parabolic filter for removal of powerline interference in ecg signal using periodogram estimation technique" 2012 International Conference on Advances in Computing and Communications. Article (CrossRef Link)

[9] J. Yi and J. Peng, "Power quality disturbances denoising using modified s-transform" Int. Conf. Sustainable Power Generation & Supply, Nanjing, China, pp. 1-5, Apr. 2009. Article (CrossRef Link)

[10] SA. Chouakri, F. Bereksi-Reguig, S. Ahmaïdi, O. Fokapu, "Wavelet Denoising of the electrocardiogram signal based on the corrupted noise estimation" IEEE Tran. Computers in Cardiology, vol. 32, pp. 1021-1024, Sep. 2005. Article (CrossRef Link)

[11] G. Kavya and V. Thulasibai, "Parabolic filter for removal of power line interference in ECG signal using periodogram estimation technique" Int. Conf. Advances Computing and Communications, Cochin, Kerala, pp. 106-109, Aug. 2012. Article (CrossRef Link)

[12] Yan Li, Baohe Yang, Zhian Wang, and Xuhui Wang, "Automatic disturbance signal monitoring method for on-line detection and recognition" 2010 International Conference On Computer Application And System Modeling (Iccasm 2010). Article (CrossRef Link)

[13] P. Pillay, A. Bhattacharjee, "Application of wavelets to model short-term power system disturbances" IEEE Tran, Power Systems, vol. 11, no. 4, pp. 2031-2037, Nov. 1996. Article (CrossRef Link)

[14] S. Santoso, E. J. Powers and W.M. Grady, "Power quality disturbance data compression using wavelets transform methods" IEEE Tran. Power Delivery, vol. 12, no. 3, pp. 1250-1257, Jul. 1997. Article (CrossRef Link)

[15] C. C. Liao, H. T. Yang and H. H. Chang, "Denoising techniques with a spatial noise-suppression method for wavelet-based power quality monitoring" IEEE Tran. Instrumentation and Measurement, vol. 60, no. 6, pp. 1986-1996, Jul. 2011. Article (CrossRef Link)

[16] C. C. Liao, "Enhanced rbf network for recognizing noise-riding power quality events" IEEE Tran. Instrumentation and Measurement, vol. 59, no. 6, pp. 1550-1561, Oct. 2010. Article (CrossRef Link)

[17] L. Lin, "Study of wavelet-based threshold de-noising for power quality signal" Int. Conf. Test and Measurement, Hong Kong, China, pp. 231-234, Dec. 2009. Article (CrossRef Link)

[18] Gu Jie, "Wavelet threshold de-noising of power quality signals", 5th Int. Conf. Natural Computation, Tianjin, China, pp.591-597, Aug. 2009. Article (CrossRef Link)

[19] H. T. Yang, "A de-noising scheme for enhancing wavelet-based power quality monitoring system" IEEE Tran. Power Delivery, vol. 16, no. 3, pp. 353-360, Jul. 2001. Article (CrossRef Link)

[20] M. A. Golroudbari, "Signal denoising based on wavelet transform using a multi-level threshold function" 7th Int. Conf. Application of Information and Communication Technologies, Baku, Azerbaijan. pp. 1-5, Oct. 2013. Article (CrossRef Link)

[21] D. L. Donoho and I. M. Johnstone, "Ideal spatial adaptation via wavelet shrinkage," Biometrika, vol. 81, pp. 425-455, 1994. Article (CrossRef Link)

[22] S. Mallat, A Wavelet Tour of Signal Processing the Sparse Way, vol. 3. 2008, p. 565-66. Article (CrossRef Link)

Muhammad Ramzan received his B.S. degree in Electrical Engineering (Power) from University of Gujrat, Pakistan, in 2012. Currently, he is doing his graduate studies in Information, Communications, and Electronics Engineering from the Catholic University of Korea (CUK), Korea. He is working as a research assistant in wireless communication lab at CUK. His research interests include power quality, denoising of signals, signal processing, wavelet transform, and smart grid applications.

Sangho Choe received the B.Sc. and the M.Sc. degree in Electronics Engineering from Hanyang University, Seoul, Korea, in 1982 and 1984, respectively, and the Ph.D. degree in electrical engineering from Texas A&M University, College Station, Texas, in 2001. He worked as a senior engineer at Agency for Defense evelopment (ADD), Taejon, Korea, from 1984 to 1994 and at Electronics Telecommunications Research Institute (ETRI), Taejon, Korea, from 1994 to 1996. During 2001 to 2002, he joined as a principal engineer at RadioCosm Inc., a silicon-valley venture company, Mountain View, CA, USA. Since March 2003, he has joined to Department of Information, Communications, and Electronics, the Catholic University of Korea, Bucheon, South Korea, where he is currently a professor. Over the years, he has served on the technical program committee of more than 50 international conferences in the wireless communications and signal processing areas. He is a member of IEEE and IEICE and a life-long member of Korean Information and Communications Society. His current research interests are in the fields of MIMO, OFDM, power signal processing, and smart grid communications.